



Evaluation of an electrochemical sensor based on gold nanoparticles supported on carbon nanofibers for detection of tartrazine dye

Andy A. Cardenas-Riojas¹ · Sandy L. Calderon-Zavaleta¹ · Ulises Quiroz-Aguinaga¹ · Elvis O. López² · Miguel Ponce-Vargas³ · Angélica M. Baena-Moncada¹

Received: 23 November 2022 / Revised: 16 January 2023 / Accepted: 21 February 2023 / Published online: 10 March 2023
© The Author(s), under exclusive licence to Springer-Verlag GmbH Germany, part of Springer Nature 2023

Abstract

An electrochemical sensor for the detection of tartrazine (Tz), a synthetic azo dye customarily found in commercial soft drinks, is herein reported. This sensor is based on a carbon paste electrode (CPE) with gold nanoparticles (AuNP) anchored in carbon nanofibers (CNF). The CNF/AuNP nanocomposite was characterized by scanning electron microscopy (SEM), energy dispersive X-Ray spectroscopy (EDS), X-ray diffraction (XRD), and electrochemical impedance spectroscopy (EIS). The electrochemical evaluation and detection of Tz was carried out by using differential pulse voltammetry (DPV) and cyclic voltammetry (CV). In terms of sensibility, the CNF/AuNP-CPE electrochemical sensor exhibits a linear range of $3.29 - 49.50 \mu\text{mol L}^{-1}$ with a coefficient of determination r^2 of 0.9946, a limit of detection (LOD) of $0.8 \pm 0.07 \mu\text{mol L}^{-1}$, and a limit of quantification (LOQ) of $2.64 \pm 0.23 \mu\text{mol L}^{-1}$. Furthermore, the proposed sensor exhibits excellent selectivity toward Tz in the presence of the sunset yellow dye, and other interferents such as sodium benzoate, NaNO_3 , NaHCO_3 , glucose and citric acid. In addition, a DFT computational study suggests that noncovalent interactions contribute to the stabilization of the Tz-AuNP assemblies at the electrode/electrolyte interface. The optimal reproducibility, repeatability, and stability during the Tz detection in commercial soft drinks makes CNF/AuNP-CPE an appealing electrode for analytical purposes.

Keywords Carbon nanofibers · Gold nanoparticles · Tartrazine · Electrochemical sensor · Differential pulse voltammetry · DFT

Introduction

Tartrazine (Tz) is a synthetic colorant commonly used in soft drinks due to its low cost and great stability under visible light, and in acidic media [1]. However, this synthetic dye must be strictly controlled by government laws due to

potential risks to human health given the presence of azo groups ($\text{R}_1\text{-N}=\text{N-R}_2$, where R_1 and R_2 can be either aryl or alkyl functional groups) susceptible to reductive cleavage leading to primary aromatic amines [2, 3]. Then, the maximum permitted level for Tz in food is 100 ppm [2, 4].

Several methods have been developed for the determination of Tz in water, such as absorption [5], photocatalytic degradation [6], HPLC [7], electroluminescence [8], etc. These methods are expensive and present a complex sample handling. Therefore, it is still a challenge to develop a sensitive and simple method for Tz determination.

In recent years, electrochemical sensors have been raising attention for dye detection due to their low cost, suitability to detect different molecules, robustness, high sensitivity, selectivity, and reproducibility [9], where the drop in the price of electrodes manufacturing can be associated to the development of new technologies involving the use of carbon nanomaterials [10] and metallic nanoparticles [11, 12]. Currently, metal nanoparticles are used to increase sensitivity in electrochemical systems taking advantage of their high

Andy A. Cardenas-Riojas, Sandy L. Calderon-Zavaleta, and Ulises Quiroz-Aguinaga these authors contributed equally to this work.

✉ Angélica M. Baena-Moncada
abaenam@uni.edu.pe

¹ Laboratorio de Investigación de Electroquímica Aplicada, Facultad de Ciencias, Universidad Nacional de Ingeniería, Av. Túpac Amaru 210, Rímac, Lima, Perú

² Department of Experimental Low Energy Physics, Brazilian Center for Research in Physics (CBPF), Rio de Janeiro 22290-180, Brazil

³ Institut de Chimie Moléculaire de Reims, UMR CNRS 7312, University of Reims Champagne-Ardenne, Moulin de La Housse, 51687 Reims, France

surface/volume ratio, which increases the electrochemically active surface area [13]. As a support for the metallic nanoparticles, several carbon-based materials have been used. Particularly, for the detection of azo dyes, multi-walled [10, 14] and single walled carbon nanotubes [15], graphene oxide [16], reduced graphene oxide [17], graphitic carbon [18], glassy carbon [19], graphite [20], hierarchical porous carbon [21], and carbon quantum dots [22] have been employed. However, to the best of our knowledge, carbon nanofibers (CNF) have not yet been used as supporting material for the electrochemical detection of food dyes.

CNF are interesting one-dimensional carbon materials widely used in solar cells and supercapacitors [23, 24]. They exhibit a unique nanofiber network structure, good conductivity and chemical stability [25]. However, they display a small surface area and a small number of active sites, resulting in a lower detection sensitivity [26, 27]. In this regard, gold nanoparticles (AuNP) are used to improve the Tz electrochemical detection of CNFs. The use of these composite nanomaterial could help to obtain low detection limits, due to the high conductivity value of the AuNP ($4 \times 10^5 \text{ S cm}^{-1}$) [28, 29], as well as the adsorbent capacity and the high surface area of CNF [30–32]. In addition, in recent years, AuNP have attracted increasing attention due to their electrocatalytic behavior leading to an improved sensitivity [33]. Moreover, AuNP-based sensors do not require the use of membranes, polymers or other materials for the formation and growth of the nanoparticle on the CNF electrode surface [34–36].

In this work a composite material based on AuNP supported on CNF is developed for the Tz electrochemical detection. This electrochemical sensor enables a rapid and high sensitivity detection of Tz in commercial drinks without a sample pretreatment, making it an appealing device for quality monitoring.

Experimental

Reagents and Solutions

All solutions were freshly prepared using deionized water (resistivity $\geq 18.2 \text{ M}\Omega \text{ cm}$ at $25 \text{ }^\circ\text{C}$) obtained from a Milli-Q purification system (Millipore). A standard solution containing 1000 mg L^{-1} of Au (HAuCl_4) in $\text{HCl } 2 \text{ mol L}^{-1}$ and potassium chloride KCl were obtained from Merck. Tz, Sodium Borohydride (NaBH_4), and iron salts 5.0 mmol L^{-1} $\text{K}_4[\text{Fe}(\text{CN})_6]/\text{K}_3[\text{Fe}(\text{CN})_6]$ were obtained from Sigma-Aldrich. Sunset yellow, sodium benzoate, NaNO_3 , NaHCO_3 , glucose and citric acid were obtained from Sigma-Aldrich and Merck, respectively. Carbon nanofibers (graphitized (iron-free), composed of conical platelets, $\text{D} \times \text{L } 100 \text{ nm} \times 20 - 200 \text{ }\mu\text{m}$) were obtained from Sigma Aldrich.

Phosphate buffer solutions of 0.1 mol L^{-1} at pH 6, 7, 8 and 9 were prepared using the salts ($\text{NaH}_2\text{PO}_4 \cdot \text{H}_2\text{O}/\text{Na}_2\text{HPO}_4 \cdot 7\text{H}_2\text{O}$, Merck). Stock solutions of $1.0 \times 10^{-2} \text{ mol L}^{-1}$ of Tz were prepared, dissolving 53.43 mg of the compound in 0.1 mol L^{-1} of phosphate buffer at pH 8.

CNF/AuNP nanocomposite synthesis

250 mg of CNF was weighed and mixed with 200 mL of $1 \times 10^{-4} \text{ mol L}^{-1}$ gold precursor standard solution at pH 9.5 (the pH was adjusted with NaOH). Then, AuNP were synthesized in situ using the procedure described in literature [37]. In the mixture, 5 mL of 0.01 mol L^{-1} NaBH_4 were added at room temperature for the formation and growth of AuNP on the CNF surface. Finally, the solution was heated to remove unreacted borohydride ions, and the composite obtained was centrifuged 3 times at 10,000 rpm in NaOH solution at pH 9.5. It was dried using an oven at $60 \text{ }^\circ\text{C}$ for 24 h. The composite obtained was CNF/AuNP.

Preparation of CNF/AuNP paste electrode

To obtain the carbon paste electrode, 1 mL of 0.05 mol L^{-1} KCl was added and carefully mixed with 100 mg of CNF/AuNP or CNF in a mortar and dried at $\sim 50 \text{ }^\circ\text{C}$ for 15 min. Afterward, 80 μL of mineral oil were added to obtain a paste. The prepared paste was then packed into the cavity of the electrode (3 mm diameter and 1.5 mm deep). The modified carbon paste electrodes (CPE) were named CNF-CPE and CNF/AuNP-CPE, respectively.

Physicochemical and Electrochemical measurements

The morphology of CNF and CNF/AuNP composite were examined using a TESCAN LYRA3 FIB-SEM. The conditions were: 25 kV, work distance of 8.5 mm and spot size of 60 μm . Energy-dispersive X-ray spectroscopy (EDS) was used to detect the AuNP in the composite at the same SEM conditions.

X-ray diffraction was used to characterize the crystalline phase and crystallite size of the samples. A PANalytical instrument Empyrean model was used to perform the measurements. The conditions were: $20^\circ \leq 2\theta \leq 70^\circ$, step size of 0.026° per each 250 s, slits of $\frac{1}{2}$ (tube) and $\frac{1}{4}$ (detector) and detector model PIXcel 3D. To determine the crystalline sizes and lattice strain of AuNP, the Williamson-Hall (W-H) method has been applied [38].

Electrochemical measurements were performed by cyclic voltammetry (CV), differential pulse voltammetry (DPV) and electrochemical impedance spectroscopy (EIS) on a Potentiostat-Galvanostat PGSTAT204 Autolab (Eco-Chemie, the Netherlands) using Nova software. Measurements were made using a glass electrochemical cell with a three-electrode

setup. A graphite bar was used as a counter electrode, and Ag/AgCl (3 mol L⁻¹ KCl) as a reference electrode.

Evaluation of CNF/AuNP/CPE sensor and the electrochemical detection of Tz

The electrochemical characterization of CNF/AuNP-CPE was performed at different pH (between 6 and 9) in presence of Tz using 0.1 mol L⁻¹ phosphate buffer solutions, by CV at a scan rate of 25 mV s⁻¹ and DPV using the following parameters: 75 mV of amplitude, 25 mV s⁻¹ of scan rate and 30 s of conditioning time. EIS analyzes were carried out in a solution of Fe²⁺/Fe³⁺ redox couple, in an electrolyte of 5.0 mmol L⁻¹ and KCl 0.1 mol L⁻¹, using a frequency range between 0.1 and 100 kHz and an amplitude of 10 mV. The Chronoamperometric and Chronocoulometric analyzes were performed by an applied potential of 0.91 V for 120 s in the absence and in the presence of Tz. CV and DPV techniques were used to evaluate the stability, reproducibility, repeatability, sensitivity, limits of detection (LOD), limits of quantification (LOQ), and selectivity of the sensor in the presence of various interferents such as: sunset yellow, sodium benzoate, NaNO₃, NaHCO₃, glucose and citric acid, during the electrochemical detection of Tz. Finally, the Tz concentration in peruvian soft drinks Inca Kola[®] and Cifrut[®] was determined by the optimized sensor, and it was validated by the UV–visible spectrophotometric technique.

Computational study of the gold-tartrazine interaction

A density functional theory (DFT) computational study has been conducted to determine the most stable array of the tartrazine molecules interacting with the gold nanoparticles at the electrode/electrolyte interface, and also to estimate the intensity of the interactions involved. The DFT calculations were carried out by using the Gaussian16 software [39], tightening self-consistent field convergence thresholds (10⁻¹⁰ a.u.), and considering a 6-311G(d)/LANL2DZ basis set and the M06-2X functional [40]. For the Au₂₀ cluster we took as a starting point the tetrahedral symmetry structure proposed by Hensen and coworkers obtained from a DFT-based genetic algorithm [41]. This structure agrees with previous quantum-chemical calculations as well as experimental IR data used to resolve the structure of neutral gas-phase gold clusters [42, 43]. The interaction energy is obtained by a fragment calculation where the gold cluster and Tz energies are subtracted from the energy of the overall system. For this calculation the counterpoise correction for the basis set superposition error is considered [44]. The solvent effects of water were included according to the Polarizable Continuum Model (PCM) [45] where the solute is placed in a cavity of molecular shape, and the solvent dielectric response is projected on the surface of the cavity.

Results and discussions

Morphological and structural evaluation of CNF/AuNP sensor

The morphologies of CNF and CNF/AuNP were explored using SEM images at different scales. Figure 1a and b show the CNF morphology, which exhibits similar features when compared with carbon nanotubes. The diameter of CNF varies between 80–110 nm, approximately. The CNF/AuNP shows a morphology similar to pure CNF (Fig. 1c and d). Through SEM, small agglomerations of AuNP between 15–25 nm of sizes were identified (Fig. 1d). Furthermore, the AuNP clusters are not distributed evenly, enabling only a qualitative elemental identification by EDS (indicated by arrows in Fig. S1).

Figure 2 shows the X-ray diffractogram of the CNF/AuNP composites. The CNF diffractogram (Fig. S2) shows a diffraction peak at 26.49° and another at 54.5°, which are consistent with the (002) and (004) plane reflections of graphite structure [46]. The crystalline structure of CNF/AuNP composite showed well-defined Bragg peaks corresponding to (111), (002) and (202) plane reflections of the Au material (face centered cubic (fcc) structure). Besides, the crystalline size of AuNP was approximately 7.5 nm, which showed a low crystalline order and low agglomeration when it is impregnated on the CNF surface (Fig. 1d) [47].

Electrochemical characterization of CNF/AuNP-CPE sensor

EIS and CV analysis were performed on CNF-CPE and CNF/AuNP-CPE (Fig. 3a and b), using the potassium hexacyanoferrate solution [Fe(CN)₆]^{3/4-} redox couple 5.0 mmol L⁻¹ and KCl 0.1 mol L⁻¹ as supporting electrolyte. EIS was evaluated to determine the electron transfer behavior of Tz. The electrochemical results are shown in Fig. 3a. The inset displays the equivalent circuit model with the following values: electrolytic support resistance (R_s), charge transfer resistance (R_{ct}), Warburg impedance (W₁ and W₂), and a phase element constant (CPE). From the Randles model it is obtained R_s = 33.5 Ω and R_{ct} = 127.6 Ω; R_s = 22.4 Ω and R_{ct} = 79.8 Ω for CNF-CPE and CNF/AuNP-CPE, respectively (Table S1). Regarding the proposed equivalent circuit, the second resistance was identified as R_{ct}. The decrease in R_{ct} is due to the presence of AuNP on the CNF surface, indicating the enhancement of electron transfer between the CNF/AuNP-CPE sensor surface and the electrolyte solution [48]. This component is confirmed by the Tafel measurement displayed in Fig. S3a. For CNF and CNF-AuNPs, 185.9 and 99.8 Ω resistances were respectively obtained. The values fit the data from impedance analysis and the

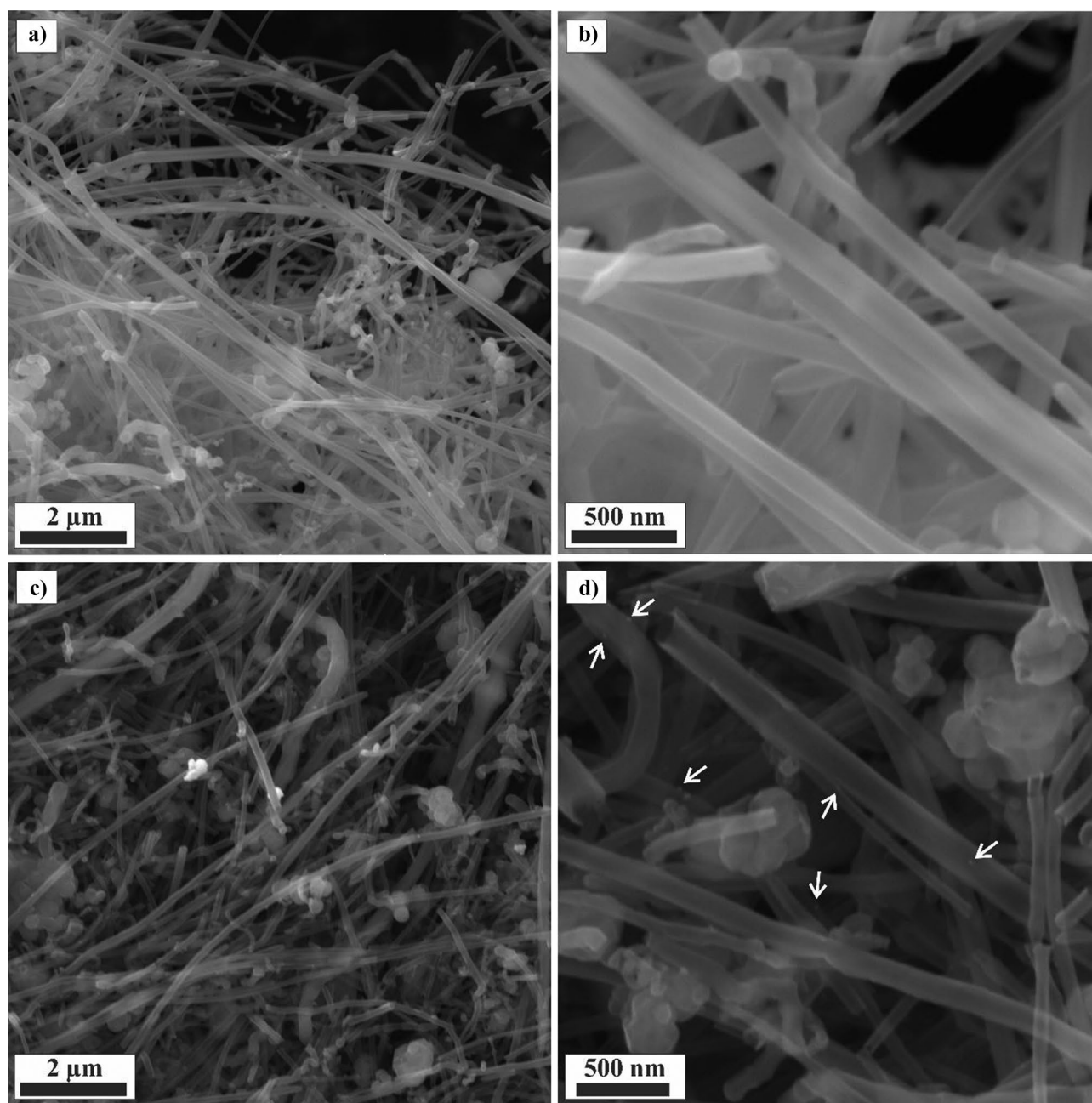


Fig. 1 SEM images for the CNF at (a) and (b) and the CNF/AuNP at (c) and (d). The AuNP are identified qualitatively from EDS as indicated with arrows at (d) image

low error percentage values in the selection of components confirm our equivalent circuit. Figure 3b shows the oxidation/reduction of the $\text{Fe}^{2+}/\text{Fe}^{3+}$ redox couple signal by CV, being sharper for the CNF/AuNP-CPE sensor. This indicates an improvement in the electron transfer and also indicates that the oxidative process between the sensor surface and the electrolyte solution is favored [49, 50].

To evaluate the transfer of electrons (k^0) on the surface of the CNF-CPE and CNF/AuNP-CPE electrodes, the estimation of the constant k^0 was made, since it is of great interest when

examining the performance of electrode materials. The rate constant provides an indication of the rate of electron transfer between an electroactive species and an electrode surface, whether the electrode material determines the overall rate of the electrochemical reaction. The value of k is obtained from Eq. 1 and Fig. S3a, where i_0 is the exchange current, n is the number of transferred electrons, F is the Faraday constant $96,485 \text{ C mol}^{-1}$, A is the electrode electroactive area in cm^2 and C the concentration of the species [51]. The value of k^0 is 4.03×10^{-6} and $7.50 \times 10^{-6} \text{ cm s}^{-1}$ for CNF-CPE and CNF/

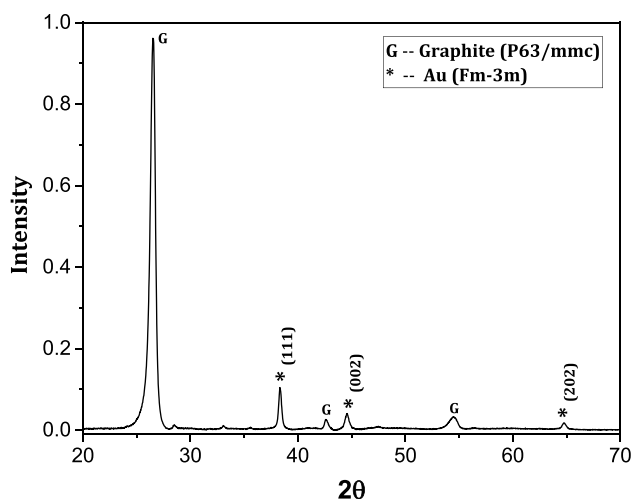


Fig. 2 X-Ray Diffraction pattern of CNF/AuNP

AuNP-CPE electrodes, respectively. These values suggest that the CNF modified with the AuNP presents a better electron transfer. The results obtained here may have a relationship with the sensitivity during Tz dye detection.

$$i_0 = nFAk^0C \quad (1)$$

The pH value of the supporting electrolyte has a significant influence on the electrochemical behavior of Tz [16]. Therefore, it is important to evaluate the optimal pH value for Tz detection. The oxidation of Tz was evaluated at different pH values in the range of 6 to 9 by DPV (Fig. 4a). The results show a potential shift to negative values when the pH for CNF/AuNP-CPE increases, as expected [16, 17]. Furthermore, the oxidation peak potential (E_{oxid}) is linear in

the pH range 6–9 (Supplementary Fig. S3). The linear equation is $E_{\text{oxid}} = 1.09 - 0.030\text{pH}$ ($r^2 = 0.9594$), and the value slope is $-30.02 \pm 3.5 \text{ mV/pH}$ [52]. These results are in good agreement to the Nernst equation (Eq. 2) of $E_{\text{pc}} = E - 0.059/n \text{ pH}$, where n is the number of transfer electrons [53, 54].

$$E_{\text{pc}} = E - \frac{0.059}{n} \text{pH} \quad (2)$$

where it can be deduced that the slope is different from the theoretical value ($30 \text{ mV} \neq 59 \text{ mV}$). These values indicate that the Tz oxidation reaction occurs via a proton with 2 transferred electrons in the process (reaction 2) [55, 56]. Furthermore, the slope -30 mV/pH indicated in Fig. S3b verifies that two electrons are transferred $n = 1.96 \sim 2$. [55, 56]. In addition, the highest Tz current oxidation intensity is observed when pH is 8. Therefore, this pH was chosen for the following experiments.

The Fig. 4b presents the electrochemical evaluation of the CNF-CPE and CNF/AuNP-CPE compounds in the presence of $9.9 \times 10^{-5} \text{ mol L}^{-1}$ Tz, with an oxidation peak at 0.86 V, for the CNF-CPE sensor modified with the AuNP, which improves the Tz electrochemical detection. After obtaining the optimal electrolyte, the DPV parameters were optimized for Tz detection. Then, the amplitude ($E_{\text{amp}} = 150 \text{ mV}$), scan rate ($v = 25 \text{ mV s}^{-1}$), accumulation potential ($E_a = 1.5 \text{ V}$) and accumulation time ($t_a = 60 \text{ s}$) were defined. [11, 57] (see Supplementary Fig. S4). The studies of the optimal parameters were carried out in the following way: The amplitude was evaluated in a range from 5 to 200 mV using a $9.9 \times 10^{-5} \text{ mol L}^{-1}$ solution of Tz while the other conditions remained constant, the results are observed in Fig S4a, where it is observed that the highest oxidation current

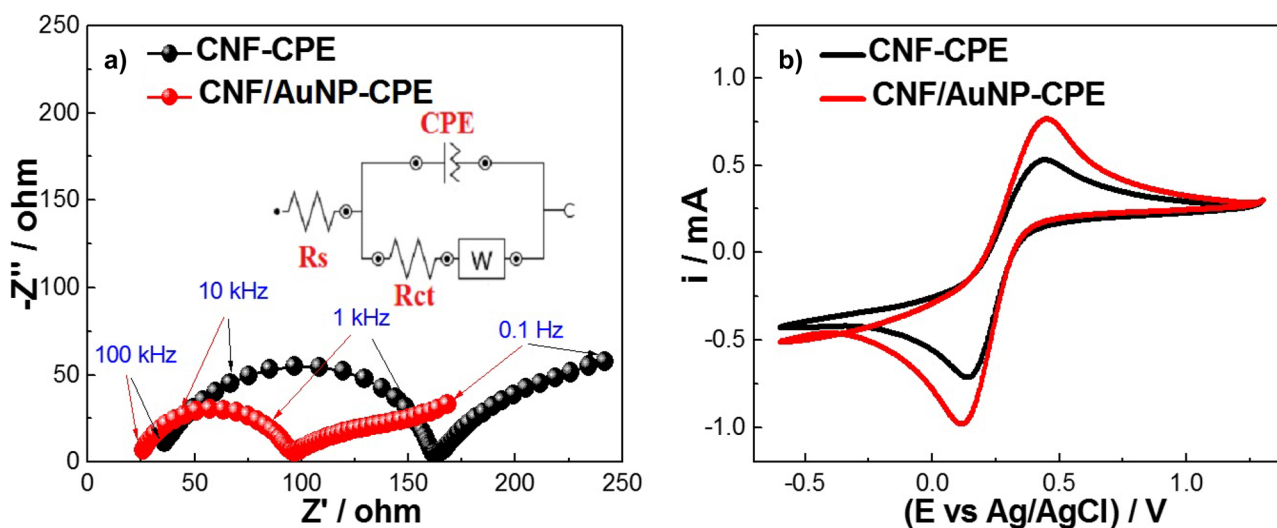


Fig. 3 a) Nyquist plot (OCP: 0.25 V), b) CV at 25 mV s^{-1} of CNF-CPE and CNF/AuNP-CPE in $5.0 \text{ mmol L}^{-1} [\text{Fe}(\text{CN})_6]^{3/4-}$ and 0.1 mol L^{-1} KCl electrolyte

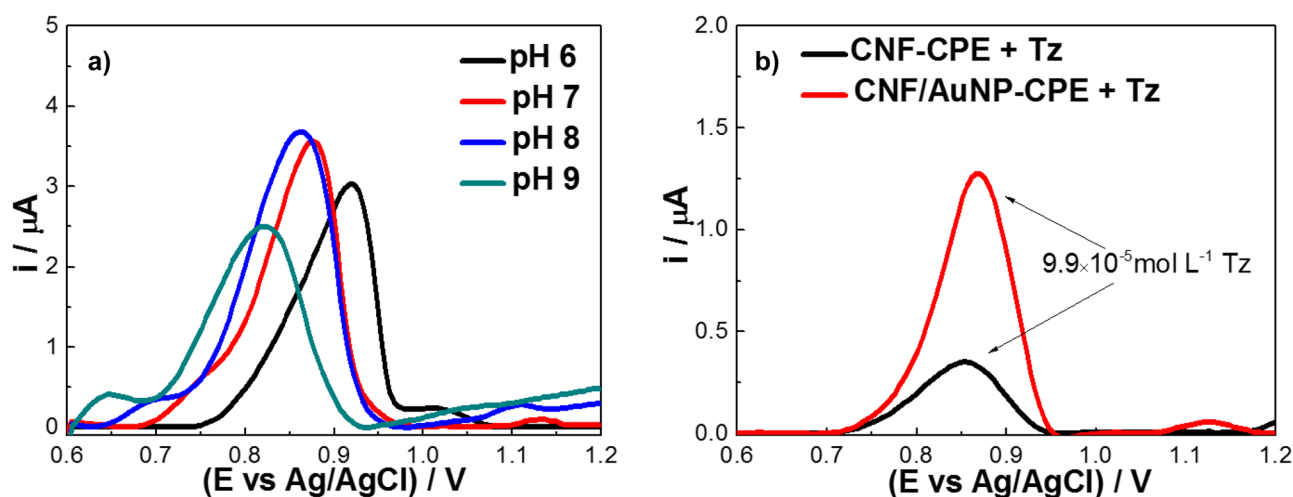
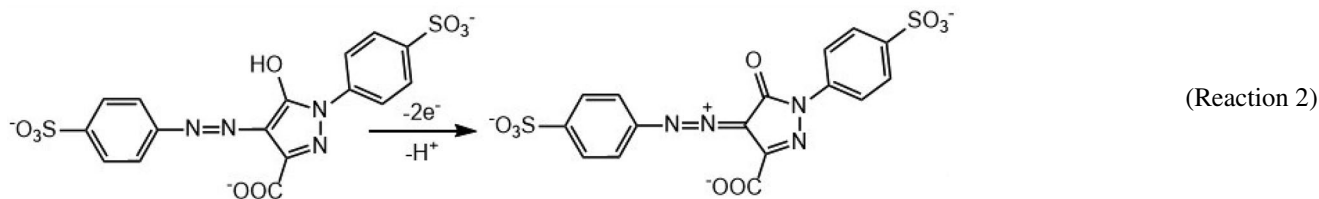


Fig. 4 DPV analysis of **a)** CNF/AuNP-CPE in phosphate buffer 0.1 mol L⁻¹ as supporting electrolyte at different pH values (6–9) in the presence of Tz 4 × 10⁻⁴ mol L⁻¹, **b)** CNF-CPE and CNF/AuNP-CPE in the presence of 9.9 × 10⁻⁵ mol L⁻¹ Tz at pH 8 at 75 mV and 25 mV s⁻¹

is obtained at 150 mV of amplitude. The same procedure was performed to obtain the optimal parameters leading to an improvement of the Tz electrochemical detection by the CNF/AuNP-CPE sensor [58]. The results are shown in Fig. S4.

attributed by the AuNP, which is related to the decreasing in the overpotential reaction on the modified electrode surface [34, 61]. The electrochemical process involved in Tz presents only one oxidation signal implying two electrons and one proton in the reaction, thus depicting an irreversible process. The electrochemical oxidation reaction of Tz is shown in reaction (2) [34, 62].



Electrochemical determination of Tz

The CVs of the CNF/AuNP-CPE sensor were recorded in absence and presence of Tz at pH = 8 in the potential range from -0.2 V to 1.3 V vs Ag/AgCl (Fig. 5). Figure 5a presents the CV of the CNF without modifying, where the oxidation potential at 1.1 V (reaction 1) and the reduction potential at 0.5 V are observed. These peaks correspond to the redox reaction of AuNP on the CNF surface according to [59, 60]:



Figure 5b shows a Tz oxidation peak at 0.9 V detected by CNF-CPE and CNF/AuNP-CPE materials [56]. The CNF-CPE material detects the Tz, through oxidation measurements. In contrast, the CNF/AuNP-CPE sensor provides well-defined signals for the anodic current of Tz. This demonstrates the synergistic effect of AuNP on CNF surface, due to the good conductivity and rapid electron transfer

Chronoamperometry is one of the electrochemical methods most commonly used to study processes in chemically modified electrodes. For example, our CNF/AuNP-CPE sensor in the detection of Tz, exhibits a potential of 0.91 V and $t = 120$ s, generating a noticeable increase in current due to the Tz molecule oxidation (Fig. 5c) [22, 34]. The inset in Fig. 5c shows the modification of those straight lines, increasing their intercept from 0.005 to 3.503 μA , due to detection of Tz by the CNF/AuNP-CPE sensor [22, 61].

Figure 5d shows the adsorbed charge by Tz on CNF/AuNP-CPE surface, determined by chronocoulometric analysis. The extrapolation of the linear slope, from the chronocoulometric test, does not pass through the origin due to the double layer charge and the oxidation reaction on Tz (Eq. 3)

$$Q = \frac{2nFAD_o^{1/2}C_o^*t^{1/2}}{\pi^{1/2}} + Q_{dl} + nFA\Gamma_o \quad (3)$$

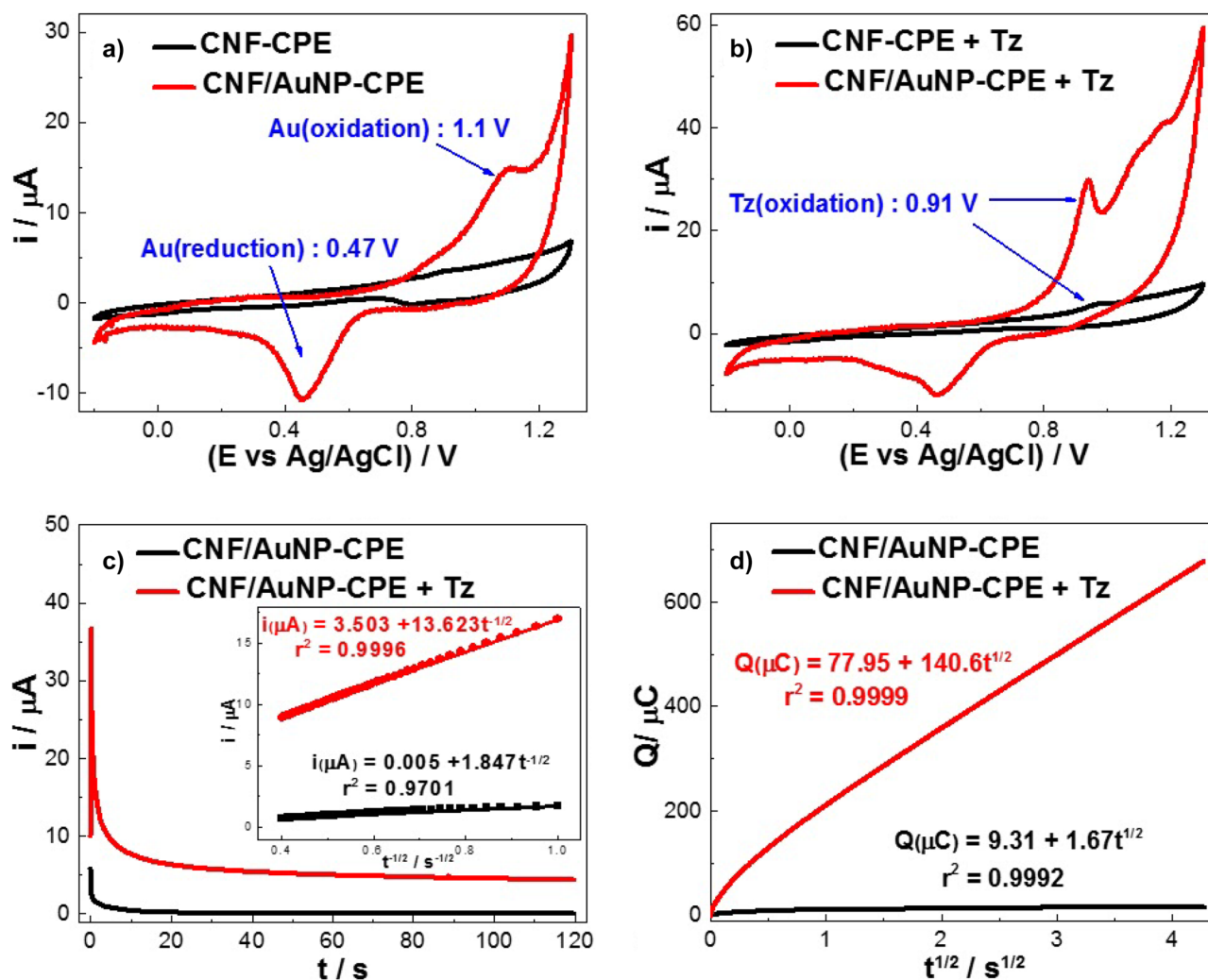


Fig. 5 Electrochemical evaluation of CNF/AuNP-CPE and CNF-CPE in a 0.1 mol L^{-1} phosphate buffer pH 8. Analysis by cyclic voltammetry a) In the absence of Tz and b) in the presence of Tz at 25 mV s^{-1} ;

where n is the stoichiometric number of electrons involved in the electrode reaction F is the Faraday constant $96,485 \text{ C mol}^{-1}$, A is the electrode electroactive area in cm^2 , D_o is the diffusion coefficient in $\text{cm}^2 \text{ s}^{-1}$, C_o^* is the concentration of the species in the solution in mol cm^{-3} , t is the time in s, Q_{dl} is the capacitive charge and Γ_o (mol cm^{-2}) is the faradaic component associated with the reduction and oxidation of the molecule adsorbed on the surface, Γ_o [63]. The charge present on the CNF/AuNP-CPE was $9.91 \mu\text{C}$ and the amount of Tz charge adsorbed on the surface of CNF/AuNP-CPE was $77.95 \mu\text{C}$ [64].

Studies of scan rate effects

The effect of different scan rates was evaluated to observe the height variation of the anodic current for Tz detected by the CNF/AuNP-CPE sensor. Fig. S5 shows the

c) chronoamperometry analysis and d) chronocoulometry analysis in the absence and in the presence of $9.9 \times 10^{-5} \text{ mol L}^{-1}$ Tz at 0.91 V during 120 s

electrochemical analysis of Tz at $9.0 \times 10^{-4} \text{ mol L}^{-1}$ by CV at different scan rates from 0.01 to 0.2 V s^{-1} . It is observed that the scan rate linearly increases with the oxidation current (ipa) (Fig. 6S). In Fig. S6a, the same behavior is observed between the maximum Tz oxidation current (ipa) and the scan rate (v), which is expressed as $\text{ipa} (\mu\text{A}) = 3.35 + 83.70v$ ($r^2 = 0.9956$), showing that the oxidation currents of Tz were enhanced with increasing scan rate from 0.01 to 0.2 V s^{-1} . A shift to more positive potentials was also observed, suggesting that the reaction mechanism of Tz at the electrode gradually changed from an absorption process to a diffusion one [11, 16]. Fig. S6b, indicates that ipa is proportional to the square root of the scan rate in the range of 0.01 to 0.2 V s^{-1} , $\text{ipa} (\mu\text{A}) = -1.75 + 4.55v^{1/2}$ ($r^2 = 0.9416$), suggesting a diffusion controlled mechanism [61]. Fig. S6c presents the linear relationship of $\text{Log}(\text{ipa})$ with $\text{Log}(v)$. The linear equation is $\text{Log}(\text{ipa}) = -4.405 + 0.510\text{Log}(v)$ ($r^2 = 0.9319$).

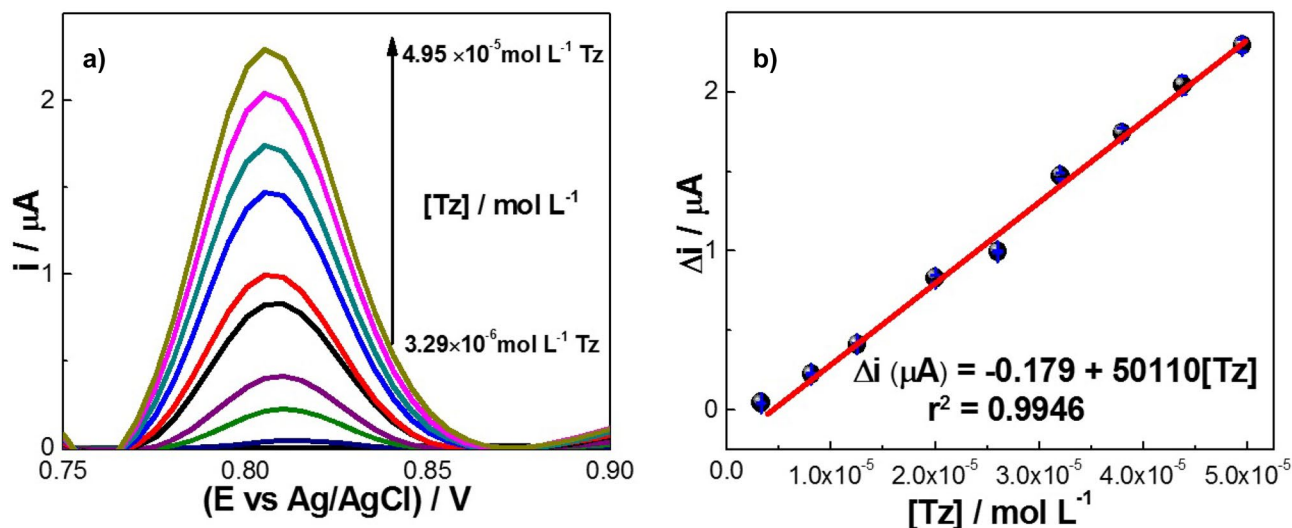


Fig. 6 a) DPV analysis of the CNF/AuNP-CPE sensor in the presence of Tz at different concentrations, in a phosphate buffer 0.1 mol L⁻¹ pH=8, at 150 mV, 25 mV s⁻¹, t_a=60 s and E_a=1.5 V b) Calibration curve of the anodic current heights as a function of Tz concentrations

The slope of the graph (Log(ip_a) vs Log(v)) is 0.51, suggesting a mixed diffusion-adsorption controlled system (slope between 0.5 and 1.0) [34, 65]. In addition, Fig. S6d presents the linear relationship between Log(ip_a) and Log(E_{pa}). The linear equation is Log(ip_a) = -3.54 + 26.58Log(E_{pa}) (r² = 0.9761) which indicates a mixed diffusion-adsorption controlled system.

Fig. S6e shows the linear relationship between E_{pa} and the logarithm of the scan rate, (Log(v)). The linear equation for this relationship is: E_{pa} = 0.925 + 0.038Log(v),

(r² = 0.9022). This indicates the irreversible nature of the electrochemical process of Tz [59]. Since the Tz reaction is an irreversible process, the number of electrons transferred in the reaction can be obtained from Eq. (4) through the difference between the E_{pa} and E_{1/2}, which corresponds to the peak current, and the half of the peak current (α = 0.50), respectively [61].

$$E_{pa} - E_{\frac{1}{2}} = \frac{0.0477}{\alpha.n} \quad (4)$$

Table 1 Comparison of different modifications of working electrodes based on carbon for Tz detection

Electrode	Technique	Linear range (μmol L ⁻¹)	LOD (μmol L ⁻¹)	Reference
CHIT/GO/MWCNTs/AuNPs/GCE	DPV	10–100 mg/mL	2735.8	[16]
Au-(AuNPs-PAH/NiTsPc) ₅	DPV	1—9	0.12	[46]
Gr-PLPA/PGE	DPV	NA	1.54	[67]
PMel/GCE	DPV	5–500	0.97	[68]
WS ₂ /DNPs/GCE	DPV	NA	4.5	[69]
SDSM/CPE	DPV	60–110	5.2	[70]
TX-100MCPE	CV	6 – 100	1.11	[71]
CHIT/CaONPs/MWCNTs/AuE	DPV	0.18 -188.7	1.69	[11]
AuNPs/PDDA-Gr/GCE	DPV	0.075 – 5.0	0.05	[72]
MWCNT-IL-CCE	DPV	3 – 70	1.10	[73]
CNF/AuNP-CPE	DPV	3.29—49.5	0.80	This work

NA Not Available, CHIT/GO/MWCNTs/AuNPs/GCE: Chitosan-graphene oxide-multiwalled carbon nanotubes modified glassy carbon electrode. Nickel(II)-phthalocyanine-tetrasulfonic (NiTsPc), the Layer-by-Layer (LbL) film was constructed following the Au-(AuNPs-PAH/NiTsPc)₅ architecture. Gr-PLPA/PGE: graphite-Poly(L-phenylalanine)-pencil graphite electrode, PGE: Pencil graphite electrode, PMel/GCE: Poly(melamine) electrodeposited on glassy carbon, WS₂/DNPs/GCE: WS₂-diamond nanoparticles modified glassy carbon electrode, SDSMCPE: Sodium dodecyl sulfate modified carbon paste electrode, TX-100MCPE: TX-100 modified carbon paste electrode, CHIT/CaONPs/MWCNTs/AuE: Chitosan-calcium nanoparticles multiwalled carbon nanotubes modified gold electrode, MWCNT-IL-CCE: multiwalled carbon nanotubes-ionic liquid-carbonceramic composite electrode. AuNPs/PDDA-Gr/GCE: Poly(diallyldimethylammoniumchloride) PDDA) functionalized gold nanoparticles/graphene(AuNPs/Gr)

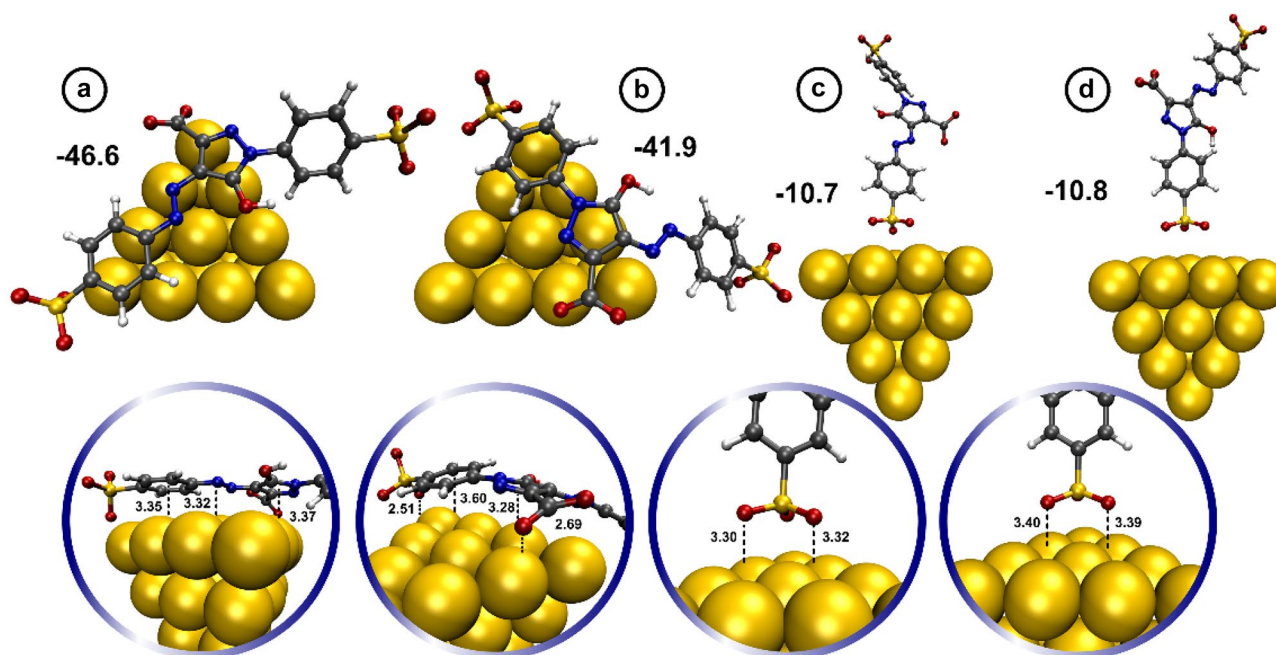


Fig. 7 Optimized geometries of Tz-AuNP systems calculated at the M06-2X/6-311G(d)/LANL2DZ level of theory. Interaction energies in kcal mol⁻¹ and interatomic distances in Angstroms

The results suggest an electron transfer process ($n = 1.94 \sim 2$) in the rate-determining step of the Tz oxidation [59].

Calibration curve and Tz detection

The electrochemical detection of Tz by the CNF/AuNP-CPE sensor was examined using DPV in a 0.1 mol L⁻¹ phosphate buffer solution at pH 8.0 under optimized experimental conditions. The results are shown in Fig. 6a, where the addition of the Tz increases the current proportionally. The results in Fig. 6b show that the oxidation current linearly increases with the concentration of Tz [66]. The calibration curve obtained for the Tz response was $\Delta i(\mu\text{A}) = -0.179 + 50110[\text{Tz}]$, with a correlation coefficient $r^2 = 0.9946$, a linear range between 3.29–49.5 $\mu\text{mol L}^{-1}$, LOD of $0.80 \pm 0.07 \mu\text{mol L}^{-1}$ and LOQ of $2.64 \pm 0.23 \mu\text{mol L}^{-1}$. These measurements were performed by triplicate. The LOD of the developed sensor was compared with different previous studies (Table 1), showing that our CNF/AuNP-CPE sensor is within the working range and within the maximum permissible limits [16].

DFT Study of the interactions between Tz and the gold nanoparticles

The tetrahedral geometry attributed to the Au₂₀ cluster has been described as a structure of face-centered cubic bulk gold, with the twenty gold atoms on its surface and each of its four faces depicting a (111) plane [40, 62]. The

constructed polyhedra is a tetrahedral pyramid with its four corners being low coordination sites. Four configurations were considered for the Tz-AuNP assemblies (See Fig. 7). The lowest energy ($-46.6 \text{ kcal mol}^{-1}$) corresponds to a Tz parallel orientation relative to an Au₂₀ face (Fig. 7a) where phenyl and pyrazole moieties interact with the gold atoms displaying averaged interatomic distances of 3.35 Å, and 3.37 Å, respectively. In this interacting assembly the nitrogen atoms of the azo group are the closest ones to Au at a distance of 3.32 Å, larger than the sum of van der Waals radii (3.21 Å) suggesting noncovalent interactions between the fragments, in line with a physisorption phenomenon. The second configuration (Fig. 7b) with the phenyl and pyrazole rings interacting with the AuNP exhibits a lower magnitude interaction energy ($-41.9 \text{ kcal mol}^{-1}$), as a consequence of the Tz bent-shaped geometry-given the contacts involving the sulfonate and carboxyl groups toward the low coordinate sites of the Au₂₀ cluster- which increases the distance between phenyl and the cluster, resulting in a less effective interaction between the fragments. As expected, lower

Table 2 Results of the RSD obtained by the reproducibility and repeatability of the sensor

# Electrodes	Reproducibility (n = 10, 4 days) / % RSD	Repeatability (n = 10) / % RSD
Electrode 1	6.95	5.69
Electrode 2	10.1	1.39
Electrode 3	8.32	2.41

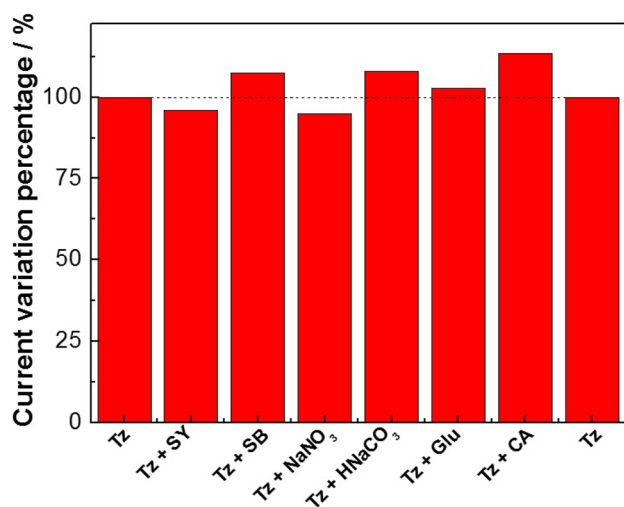


Fig. 8 DPV analysis of the CNF/AuNP-CPE sensor in the presence of different interferents in phosphate buffer 0.1 mol L^{-1} pH=8, at 150 mV , 25 mV s^{-1} , $t_a = 60 \text{ s}$ and $E_a = 1.5 \text{ V}$

interaction energies (about 11 kcal mol^{-1}) are found for the side-to-face binding modes (Fig. 7c and d), where the Tz sulfonate groups interact with the central Au atoms of the cluster face. In summary, DFT calculations reveal that a parallel orientation of the Tz molecule with respect to the surface of Au_{20} is favored, with interatomic distances suggesting a

physisorption at the electrode-solution interface of the CNF/AuNP-CPE sensor.

Study of the reproducibility, repeatability and selectivity of the CNF/AuNP-CPE sensor

Repeatability and reproducibility analysis of the CNF/AuNP-CPE sensor by DPV using a Tz concentration of $4.75 \times 10^{-4} \text{ mol L}^{-1}$ in a phosphate buffer solution of 0.1 mol L^{-1} at pH 8.0 and using 3 different electrodes, were performed by 10 consecutive measurements ($n = 10$) in 4 different days. The application of the analytical method yielded a relative standard deviation (RSD) lower than 10%, as shown in Table 2. The results obtained showed that the proposed method exhibits an excellent precision when applied for Tz dye detection.

The selectivity analysis of the proposed sensor was performed in the presence of the following interferents: sunset yellow (SY), sodium benzoate (SB), NaNO_3 , NaHCO_3 , glucose (Glu) and citric acid (CA) at a concentration of $1 \times 10^{-4} \text{ mol L}^{-1}$ in a phosphate buffer 0.1 mol L^{-1} of pH 8 in presence of $4.75 \times 10^{-4} \text{ mol L}^{-1}$ of Tz. Figure 8 presents the current variation percentage due to the interfering species presence. The percentage of relative standard deviation (%RSD) varies from 94.8 to 113.5%, implying that the CNF/AuNP-CPE sensor is selective. This demonstrates that the CNF/AuNP-CPE sensor can be successfully applied for Tz dye detection in the presence of the aforementioned interfering compounds.

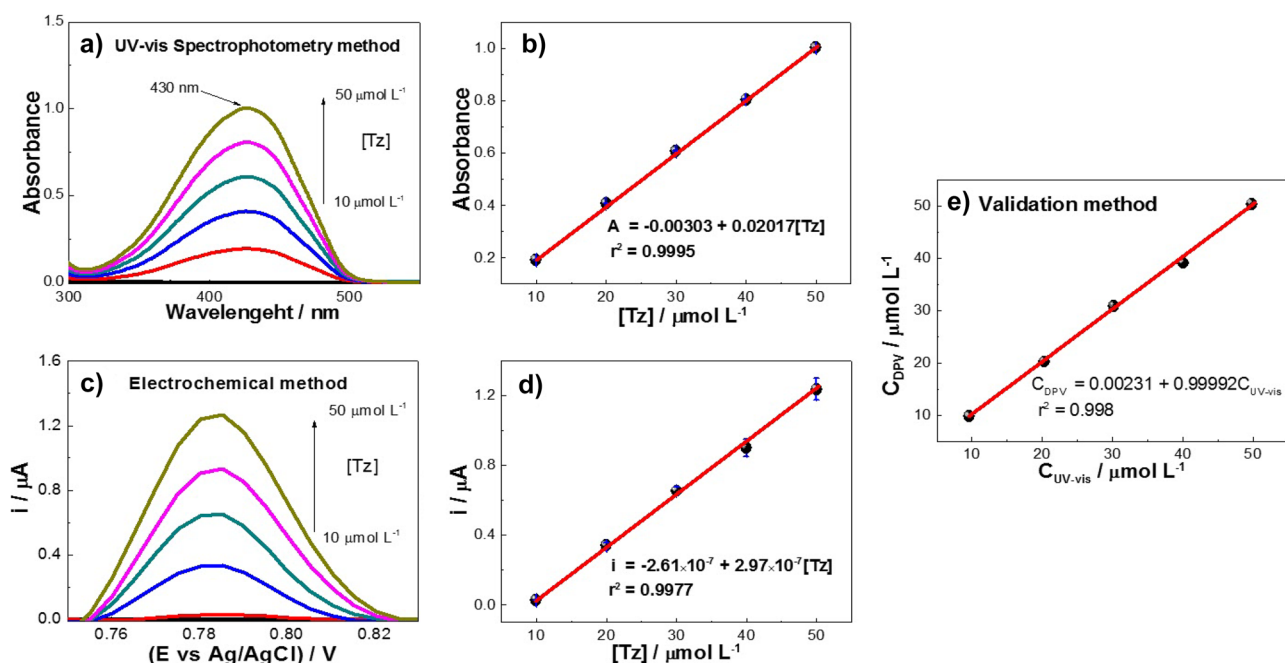


Fig. 9 Analysis of Tz in synthetic samples using a), b) the UV–visible spectrophotometric method and calibration curve; c), d) the electrochemical method and calibration curve and e) Validation of the electrochemical method

Table 3 Analysis of Tz in synthetic samples using the electrochemical method and the UV–visible spectrophotometric method

Concentration of Tz added ($\mu\text{mol L}^{-1}$)	Tz detected by electrochemical method ($\mu\text{mol L}^{-1}$)	Recovered (%)	Tz detected by UV–visible spectrophotometric ($\mu\text{mol L}^{-1}$)	Recovered (%)
10	9.72	97.20	9.63	96.63
20	20.19	100.95	20.32	101.60
30	30.73	102.43	30.22	100.73
40	39.03	97.57	40.01	100.02
50	50.30	100.60	49.79	99.58

Validation of the electrochemical method by UV–visible spectrophotometry

Our sensor was validated using an UV–Vis analysis, and it was used as a comparative method for Tz quantification in synthetic and real samples. First, a calibration curve for Tz was constructed by the UV–visible technique in the same linear concentration range used for the DPV electrochemical technique (Fig. 9 and Table 3).

Figure 9a presents a maximum absorbance around 430 nm of Tz [50, 74, 75]. From this UV–vis spectrum, an analytical curve was obtained, which exhibits a linear behavior with $r^2=0.9995$ in the concentration range between 10.0 to 50.0 $\mu\text{mol L}^{-1}$ of Tz, from the following equation: $A = -0.00303 + 0.02017[\text{Tz}]$ (Fig. 9b). In the same way, as observed in Fig. 9c, the electrode was analyzed by DPV with a concentration range between 10.0 to 50.0 $\mu\text{mol L}^{-1}$ of Tz, obtaining the following equation: $\Delta i = -2.61 \times 10^{-7} + 2.97 \times 10^{-7}[\text{Tz}]$, and a linear behavior with $r^2 = 0.9977$ (Fig. 9d).

Since the DPV method was evaluated at different levels of Tz concentration in synthetic samples. These results are compared with those obtained by the spectrophotometric method (Fig. 9e). The DPV validation by the spectrophotometric method was carried out by simple linear regression, obtaining a high coefficient of determination value (r^2) of 0.998, where the high percentage of the data is explained with the adjusted linear regression model: $C_{\text{DPV}} = 0.002 + 0.999 C_{\text{UV-vis}}$. In addition, the linear regression slope presents an upper and lower confidence limits of +1.071 and -0.928, respectively, where the obtained slope value is in good agreement with the ideal value of 1.0 for this model. On the other hand, the upper and lower confidence

limits for the intercept are +2.361 and -2.357, respectively. The values include the ideal value of zero, with a confidence level of 95%. Therefore, from the results is concluded that the spectrometric method is a useful analytical technique to validate the DPV analysis. The CNF/AuNP-CPE electrochemical sensor provides reliability and good accuracy for a wide range of Tz concentrations [49, 76]. The results of the analysis of the real sample are indicated in Table 4, evaluating the Inca Kola[®] and Cifrut[®] soft drinks.

Conclusion

A new electrochemical sensor based on carbon nanofibers modified with AuNP was developed for Tz dye detection. The morphology of the AuNP on the surface of the CNF was observed by SEM. The crystallite size of the AuNP (face centered cubic structure) ranges between 15 and 20 nm. The CNF/AuNP-CPE presents excellent stability, reproducibility and repeatability, with linear a range between 3.29–49.5 $\mu\text{mol L}^{-1}$, with $r^2 = 0.9946$, with a low detection limit of $0.80 \pm 0.07 \mu\text{mol L}^{-1}$ and a limit of quantification of $2.64 \pm 0.23 \mu\text{mol L}^{-1}$. The robustness of the sensor selectivity in the presence of various interfering species (sunset yellow, sodium benzoate, NaNO_3 , NaHCO_3 , glucose and citric acid) has been demonstrated. DFT calculations in a PCM solvent model reveal that a parallel orientation of Tz relative to the Au_{20} surface is favored, where the interatomic distances involved suggest a physisorption phenomenon at the electrode-solution interface. Finally, the CNF/AuNP-CPE sensor exhibits a rapid response, making it an appealing analytical tool for the detection and quantification of Tz dye in soft drinks.

Table 4 Analysis of Tz in soft drinks using the electrochemical method and the UV–visible spectrophotometric method

# Soft drinks	Tz detected by electrochemical method ($\mu\text{mol L}^{-1}$)	Tz detected by UV–visible spectrophotometric ($\mu\text{mol L}^{-1}$)
Cifrut	16.99	16.77
Inca Kola	47.59	47.60

Supplementary Information The online version contains supplementary material available at <https://doi.org/10.1007/s10008-023-05438-5>.

Acknowledgements The authors gratefully acknowledge the Laboratorio de Investigación de Electroquímica Aplicada, Facultad de Ciencias de la Universidad Nacional de Ingeniería Lima-Peru. The authors wish to thank the Department of Experimental Low Energy Physics, Brazilian Center for Research in Physics (CBPF) for the use of SEM and XRD equipment. The authors acknowledge the Centre de Calcul Régional ROMEO, France for computing facilities (<http://romeo.univ-reims.fr>).

Declarations

Conflicts of interest There are no conflicts of interest.

References

- Rodríguez JA, Juárez MG, Galán-Vidal CA et al (2015) Determination of Allura Red and Tartrazine in Food Samples by Sequential Injection Analysis Combined with Voltammetric Detection at Antimony Film Electrode. *Electroanalysis* 27:2329–2334. <https://doi.org/10.1002/elan.201500295>
- Darabi R, Shabani-Nooshabadi M (2021) NiFe₂O₄-rGO/ionic liquid modified carbon paste electrode: An amplified electrochemical sensitive sensor for determination of Sunset Yellow in the presence of Tartrazine and Allura Red. *Food Chem* 339:127841. <https://doi.org/10.1016/j.foodchem.2020.127841>
- Lipskikh OI, Korotkova EI, Khristunova YP et al (2018) Sensors for voltammetric determination of food azo dyes - A critical review. *Electrochim Acta* 260:974–985
- Chao M, Ma X (2015) Convenient Electrochemical Determination of Sunset Yellow and Tartrazine in Food Samples Using a Poly(L-Phenylalanine)-Modified Glassy Carbon Electrode. *Food Anal Methods* 8:130–138. <https://doi.org/10.1007/s12161-014-9879-6>
- Chukwumeka-Okorie HO, Ekuma FK, Akpomie KG et al (2021) Adsorption of tartrazine and sunset yellow anionic dyes onto activated carbon derived from cassava sievate biomass. *Appl Water Sci* 11:27. <https://doi.org/10.1007/s13201-021-01357-w>
- Rashidi M, Sajjadi SM, Mousavi HZ (2019) Kinetic analysis of azo dye decolorization during their acid–base equilibria: photocatalytic degradation of tartrazine and sunset yellow. *React Kinet Mech Catal* 128:555–570. <https://doi.org/10.1007/s11144-019-01654-1>
- Alp H, Başkan D, Yaşar A et al (2018) Simultaneous determination of sunset yellow FCF, allura red AC, quinoline yellow WS, and tartrazine in food samples by RP-HPLC. *J Chem*. <https://doi.org/10.1155/2018/6486250>
- Niu H, Yang X, Wang Y et al (2020) Electrochemiluminescence Detection of Sunset Yellow by Graphene Quantum Dots. *Front Chem* 8:505. <https://doi.org/10.3389/fchem.2020.00505>
- Sun SC, Hsieh BC, Chuang MC (2019) Electropolymerised-hemin-catalysed reduction and analysis of tartrazine and sunset yellow. *Electrochim Acta* 319:766–774. <https://doi.org/10.1016/j.electacta.2019.07.014>
- Qiu X, Lu L, Leng J et al (2016) An enhanced electrochemical platform based on graphene oxide and multi-walled carbon nanotubes nanocomposite for sensitive determination of Sunset Yellow and Tartrazine. *Food Chem* 190:889–895. <https://doi.org/10.1016/j.foodchem.2015.06.045>
- Rovina K, Siddiquee S, Shaarani SM (2017) Highly sensitive electrochemical determination of sunset yellow in commercial food products based on CHIT/GO/MWCNTs/AuNPs/GCE. *Food Control* 82:66–73. <https://doi.org/10.1016/j.foodcont.2017.06.029>
- Qin C, Guo W, Liu Y et al (2017) A Novel Electrochemical Sensor Based on Graphene Oxide Decorated with Silver Nanoparticles-Molecular Imprinted Polymers for Determination of Sunset Yellow in Soft Drinks. *Food Anal Methods* 10:2293–2301. <https://doi.org/10.1007/s12161-016-0753-6>
- Fang C, Dharmarajan R, Megharaj M, Naidu R (2017) Gold nanoparticle-based optical sensors for selected anionic contaminants. *TrAC - Trends Anal Chem* 86:143–154
- Zhao L, Zeng B, Zhao F (2014) Electrochemical determination of tartrazine using a molecularly imprinted polymer – multiwalled carbon nanotubes - ionic liquid supported Pt nanoparticles composite film coated electrode. *Electrochim Acta* 146:611–617. <https://doi.org/10.1016/J.ELECTACTA.2014.08.108>
- Nuñez-Dallos N, Macías MA, OlimpoGarcía-Beltrán et al (2018) Voltammetric determination of amaranth and tartrazine with a new double-stranded copper(I) helicate-single-walled carbon nanotube modified screen printed electrode. *J Electroanal Chem* 822:95–104. <https://doi.org/10.1016/J.JELECHEM.2018.05.017>
- Rovina K, Siddiquee S, Shaarani SM (2019) An electrochemical sensor for the determination of tartrazine based on CHIT/GO/MWCNTs/AuNPs composite film modified glassy carbon electrode. 44:447–457. <https://doi.org/10.1080/01480545.2019.1601210>
- He Q, Liu J, Liu X et al (2018) Sensitive and Selective Detection of Tartrazine Based on TiO₂-Electrochemically Reduced Graphene Oxide Composite-Modified Electrodes. *Sensors* 18:1911. <https://doi.org/10.3390/S18061911>
- Karimi MA, Aghaei VH, Nezhadali A (2018) Graphitic Carbon Nitride as a New Sensitive Material for Electrochemical Determination of Trace Amounts of Tartrazine in Food Samples. *Food Anal Methods* 11(11):2907–2915. <https://doi.org/10.1007/S12161-018-1264-4>
- Ye X, Du Y, Lu D, Wang C (2013) Fabrication of β-cyclodextrin-coated poly (diallyldimethylammonium chloride)-functionalized graphene composite film modified glassy carbon-rotating disk electrode and its application for simultaneous electrochemical determination colorants of sunset yellow. *Anal Chim Acta* 779:22–34. <https://doi.org/10.1016/J.ACA.2013.03.061>
- de Lima LF, Ferreira AL, Maciel CC et al (2021) Disposable and low-cost electrochemical sensor based on the colorless nail polish and graphite composite material for tartrazine detection. *Talanta* 227:122200. <https://doi.org/10.1016/J.TALANTA.2021.122200>
- An ZZ, Li Z, Guo YY et al (2017) Preparation of chitosan/N-doped graphene natively grown on hierarchical porous carbon nanocomposite as a sensor platform for determination of tartrazine. *Chinese Chem Lett* 28:1492–1498. <https://doi.org/10.1016/J.CCLET.2017.02.014>
- Mehmandoust M, Erk N, Karaman O et al (2021) Three-dimensional porous reduced graphene oxide decorated with carbon quantum dots and platinum nanoparticles for highly selective determination of azo dye compound tartrazine. *Food Chem Toxicol* 158:112698. <https://doi.org/10.1016/J.FCT.2021.112698>
- Wu Y, Ran F (2017) Vanadium nitride quantum dot/nitrogen-doped microporous carbon nanofibers electrode for high-performance supercapacitors. *J Power Sources* 344:1–10. <https://doi.org/10.1016/j.jpowsour.2017.01.095>
- Lu N, Shao C, Li X et al (2016) CuO nanoparticles/nitrogen-doped carbon nanofibers modified glassy carbon electrodes for non-enzymatic glucose sensors with improved sensitivity. *Ceram Int* 42:11285–11293. <https://doi.org/10.1016/j.ceramint.2016.04.046>
- Guo C, Hu M, Li Z et al (2020) Structural hybridization of bimetallic zeolitic imidazolate framework (ZIF) nanosheets and carbon nanofibers for efficiently sensing α-synuclein oligomers. *Sensors Actuators B Chem* 309:127821. <https://doi.org/10.1016/j.snb.2020.127821>
- Park J, Eun C (2016) Electrochemical Behavior and Determination of Salicylic Acid at Carbon-fiber Electrodes. *Electrochim Acta* 194:346–356. <https://doi.org/10.1016/j.electacta.2016.02.103>
- Yue HY, Wu PF, Huang S et al (2019) Golf ball-like MoS₂ nanosheet arrays anchored onto carbon nanofibers for electrochemical detection of dopamine. *Microchim Acta* 186:1–7. <https://doi.org/10.1007/s00604-019-3495-5>
- Chen M, Zhou X, Liu X et al (2018) Facilitated extracellular electron transfer of *Geobacter sulfurreducens* biofilm with in situ formed gold nanoparticles. *Biosens Bioelectron* 108:20–26. <https://doi.org/10.1016/J.BIOS.2018.02.030>
- Park K, Seo D, Lee J (2008) Conductivity of silver paste prepared from nanoparticles. *Colloids Surfaces A Physicochem Eng Asp* 313–314:351–354. <https://doi.org/10.1016/J.COLSURFA.2007.04.147>

30. Li P, Huang D, Huang J et al (2020) Development of magnetic porous carbon nano-fibers for application as adsorbents in the enrichment of trace Sudan dyes in foodstuffs. *J Chromatogr A* 1625:461305. <https://doi.org/10.1016/j.chroma.2020.461305>
31. Widiyastuti W, Fahrudin Rois M, Suari NMIP, Setyawan H (2020) Activated carbon nanofibers derived from coconut shell charcoal for dye removal application. *Adv Powder Technol* 31:3267–3273. <https://doi.org/10.1016/J.APT.2020.06.012>
32. Mody VV, Siwale R, Singh A, Mody HR (2010) Introduction to metallic nanoparticles. *J Pharm Bioallied Sci* 2:282. <https://doi.org/10.4103/0975-7406.72127>
33. Khan SB, Maqsood A, Ganash A et al (2022) Development of a Novel Electrochemical Sensor Based on Gold Nanoparticle-Modified Carbon-Paste Electrode for the Detection of Congo Red Dye. *Mol* 28:19. <https://doi.org/10.3390/MOLECULES28010019>
34. Ghoreishi SM, Behpour M, Golestaneh M (2012) Simultaneous determination of Sunset yellow and Tartrazine in soft drinks using gold nanoparticles carbon paste electrode. *Food Chem* 132:637–641. <https://doi.org/10.1016/J.FOODCHEM.2011.10.103>
35. State RG, van Staden J (Koo) F, State RN, Papa F (2022) Rapid and sensitive electrochemical determination of tartrazine in commercial food samples using IL/AuTiO₂/GO composite modified carbon paste electrode. *Food Chem* 385:132616. <https://doi.org/10.1016/J.FOODCHEM.2022.132616>
36. Figueira Alves G, Vinícius de Faria L, Pedrosa Lisboa T et al (2022) A portable and affordable paper electrochemical platform for the simultaneous detection of sunset yellow and tartrazine in food beverages and desserts. *Microchem J* 181:107799. <https://doi.org/10.1016/J.MICROC.2022.107799>
37. Calderon SL, Avelino PG, Baena-Moncada AM et al (2020) Electrical energy generation in a double-compartment microbial fuel cell using *Shewanella* spp. strains isolated from Odontesthes regia. *Sustain Environ Res* 30:31. <https://doi.org/10.1186/s42834-020-00073-5>
38. Yogamalar R, Srinivasan R, Vinu A et al (2009) X-ray peak broadening analysis in ZnO nanoparticles. *Solid State Commun* 149:1919–1923. <https://doi.org/10.1016/J.SSC.2009.07.043>
39. Gaussian 16, Revision C.01, Frisch MJ, Trucks GW, Schlegel HB, Scuseria GE, Robb MA, Cheeseman JR, Scalmani G, Barone V, Petersson GA, Nakatsuji H, Li X, Caricato M, Marenich AV, Bloino J, Janesko BG, Gompers (2016) No Title
40. Zhao Y, Truhlar DG (2008) The M06 suite of density functionals for main group thermochemistry, thermochemical kinetics, non-covalent interactions, excited states, and transition elements: two new functionals and systematic testing of four M06-class functionals and 12 other function. *Theor Chem Acc* 120:215–241
41. Liu JX, Filot IAW, Su Y et al (2018) Optimum Particle Size for Gold-Catalyzed CO Oxidation. *J Phys Chem C* 122:8327–8340. <https://doi.org/10.1021/acs.jpcc.7b12711>
42. Li Z, Chen H-YT, Schouteden K et al (2020) Unraveling the atomic structure, ripening behavior, and electronic structure of supported Au₂₀ clusters. *Sci Adv* 6. <https://doi.org/10.1126/sciadv.aay4289>
43. Li J, Li X, Zhai H-J, Wang L-S (2003) Au₂₀: A Tetrahedral Cluster. *Science* (80-) 299:864–867. <https://doi.org/10.1126/science.1079879>
44. Boys SF, Bernardi F (1970) The calculation of small molecular interactions by the differences of separate total energies. Some procedures with reduced errors. *Mol Phys* 19(4):553–66
45. Mennucci B, Tomasi J, Cammi R et al (2002) Polarizable continuum model (PCM) calculations of solvent effects on optical rotations of chiral molecules. *J Phys Chem A* 106:6102–6113
46. He Z, Li M, Li Y et al (2018) Flexible electrospun carbon nanofiber embedded with TiO₂ as excellent negative electrode for vanadium redox flow battery. *Electrochim Acta* 281:601–610. <https://doi.org/10.1016/J.ELECTACTA.2018.06.011>
47. Karra S, Wooten M, Griffith W, Gorski W (2016) Morphology of Gold Nanoparticles and Electrocatalysis of Glucose Oxidation. *Electrochim Acta* 218:8–14. <https://doi.org/10.1016/J.ELECTACTA.2016.09.097>
48. Cárdenas Riojas AA, Wong A, Planes GA et al (2019) Development of a new electrochemical sensor based on silver sulfide nanoparticles and hierarchical porous carbon modified carbon paste electrode for determination of cyanide in river water samples. *Sensors Actuators B Chem* 287:544–550. <https://doi.org/10.1016/J.SNB.2019.02.053>
49. Li Z, Cheng Y-H, Feng L et al (2019) Communication—Electrochemical Impedance Signature of a Non-Planar, Interdigitated, Flow-Through, Porous, Carbon-Based Microelectrode. *J Electrochem Soc* 166:B1669–B1672. <https://doi.org/10.1149/2.0041916JES/XML>
50. de Lima LF, Ferreira AL, Maciel CC et al (2021) Disposable and low-cost electrochemical sensor based on the colorless nail polish and graphite composite material for tartrazine detection. *Talanta* 227:122200. <https://doi.org/10.1016/J.TALANTA.2021.122200>
51. Randviir EP (2018) A cross examination of electron transfer rate constants for carbon screen-printed electrodes using Electrochemical Impedance Spectroscopy and cyclic voltammetry. *Electrochim Acta* 286:179–186. <https://doi.org/10.1016/J.ELECTACTA.2018.08.021>
52. Manjunatha JG, Deraman M, Basri NH, Talib IA (2018) Fabrication of poly (Solid Red A) modified carbon nano tube paste electrode and its application for simultaneous determination of epinephrine, uric acid and ascorbic acid. *Arab J Chem* 11:149–158. <https://doi.org/10.1016/J.ARABJC.2014.10.009>
53. Scholz F (2017) Wilhelm Ostwald's role in the genesis and evolution of the Nernst equation. *J Solid State Electrochem* 21:1847–1859. <https://doi.org/10.1007/S10008-017-3619-Y/METRICS>
54. Zhou C, Liu Z, Dong Y, Li D (2009) Electrochemical Behavior of o-Nitrophenol at Hexagonal Mesoporous Silica Modified Carbon Paste Electrodes. *Electroanalysis* 21:853–858. <https://doi.org/10.1002/ELAN.200804480>
55. Lu Y, Bao C, Zou J et al (2022) Highly Sensitive Electrochemical Sensor for Sunset Yellow Based on Electrochemically Activated Glassy Carbon Electrode. *Mol* 2022, Vol 27, Page 5221 27:5221. <https://doi.org/10.3390/MOLECULES27165221>
56. Li J, Kuang D, Feng Y et al (2012) A graphene oxide-based electrochemical sensor for sensitive determination of 4-nitrophenol. *J Hazard Mater* 201–202:250–259. <https://doi.org/10.1016/J.JHAZMAT.2011.11.076>
57. Wang M, Zhao J (2015) Facile synthesis of Au supported on ionic liquid functionalized reduced graphene oxide for simultaneous determination of Sunset yellow and Tartrazine in drinks. *Sensors Actuators B Chem* 216:578–585. <https://doi.org/10.1016/J.SNB.2015.04.053>
58. Durigon AMM, da Silveira GD, Sokal FR et al (2020) Food dyes screening using electrochemistry approach in solid state: the case of sunset yellow dye electrochemical behavior. *J Solid State Electrochem* 24:2907–2921. <https://doi.org/10.1007/S10008-020-04678-Z/METRICS>
59. Bond AM, Kratsis S, Mitchell S, Mocak J (1997) Comparison of the Gold Reduction and Stripping Processes at Platinum, Rhodium, Iridium, Gold and Glassy Carbon Micro- and Macrodisks Electrodes. *Analyst* 122:1147–1152. <https://doi.org/10.1039/A702632C>
60. Elemike EE, Onwudiwe DC, Fayemi OE (2019) Botha TL (2019) Green synthesis and electrochemistry of Ag, Au, and Ag–Au bimetallic nanoparticles using golden rod (*Solidago canadensis*) leaf extract. *Appl Phys A* 125(125):1–12. <https://doi.org/10.1007/S00339-018-2348-0>
61. Karim-Nezhad G, Khorablou Z, Zamani M et al (2017) Voltammetric sensor for tartrazine determination in soft drinks using poly (p-aminobenzenesulfonic acid)/zinc oxide nanoparticles in carbon

- paste electrode. *J Food Drug Anal* 25:293–301. <https://doi.org/10.1016/J.JFDA.2016.10.002>
62. Ascencio-Flores YF, Carhuayal-Alvarez SM, Quiroz-Aguinaga U et al (2022) Simultaneous square wave voltammetry detection of azo dyes using silver nanoparticles assembled on carbon nanofibers. *Electrochim Acta* 141:782. <https://doi.org/10.1016/J.ELECTACTA.2022.141782>
 63. Bard AJ, Faulkner LR (2000) *Electrochemical Methods: Fundamentals and Applications*, 2nd edn. Wiley
 64. Ji L, Cheng Q, Wu K, Yang X (2016) Cu-BTC frameworks-based electrochemical sensing platform for rapid and simple determination of Sunset yellow and Tartrazine. *Sensors Actuators, B Chem* 231:12–17. <https://doi.org/10.1016/j.snb.2016.03.012>
 65. Wong A, Santos AM, Cardenas-Riojas AA et al (2022) Voltammetric sensor based on glassy carbon electrode modified with hierarchical porous carbon, silver sulfide nanoparticles and fullerene for electrochemical monitoring of nitrite in food samples. *Food Chem* 383:132384. <https://doi.org/10.1016/J.FOODCHEM.2022.132384>
 66. Mazlan SZ, Lee YH, Hanifah SA (2017) A New Laccase Based Biosensor for Tartrazine. *Sensors* 2017, Vol 17, Page 2859 17:2859. <https://doi.org/10.3390/S17122859>
 67. Tahtaisleyen S, Gorduk O, Sahin Y (2020) Electrochemical Determination of Tartrazine Using a Graphene/Poly(L-Phenylalanine) Modified Pencil Graphite Electrode. <https://doi.org/10.1080/00032719.2020.1716242>
 68. Wu S, Yin ZZ, Chen X et al (2020) Electropolymerized melamine for simultaneous determination of nitrite and tartrazine. *Food Chem* 333:127532. <https://doi.org/10.1016/J.FOODCHEM.2020.127532>
 69. Blanco E, Arias L, Vázquez L et al (2020) Sensor based on diamond nanoparticles and WS2 for ponceau 4R and tartrazine determination: Influence of green solvents employed for WS2 exfoliation. *FlatChem* 23:100185. <https://doi.org/10.1016/J.FLATC.2020.100185>
 70. Raril C, Manjunatha JG (2021) Development of sodium dodecyl sulfate based electrochemical sensor for tartrazine determination. *Port Electrochim Acta* 39:59–70. <https://doi.org/10.4152/PEA.202101059>
 71. (PDF) Fabrication of the Tartrazine Voltammetric Sensor based on Surfactant Modified Carbon Paste Electrode
 72. Wu T, Wang Q, Peng XY, Guo Y (2022) Facile Synthesis of Gold/Graphene Nanocomposites for Simultaneous Determination of Sunset Yellow and Tartrazine in Soft Drinks. *Electroanalysis* 34:83–90. <https://doi.org/10.1002/ELAN.202100464>
 73. Majidi MR (2012) Fadakar Bajeh Baj R, Naseri A (2012) Carbon Nanotube-Ionic Liquid (CNT-IL) Nanocomposite Modified Sol-Gel Derived Carbon-Ceramic Electrode for Simultaneous Determination of Sunset Yellow and Tartrazine in Food Samples. *Food Anal Methods* 65(6):1388–1397. <https://doi.org/10.1007/S12161-012-9556-6>
 74. Floriano L, Ribeiro LC, Saibt N (2018) Determination of Six Synthetic Dyes in Sports Drinks by Dispersive Solid-Phase Extraction and HPLC-UV-Vis. *J Braz Chem Soc* 29:602–608. <https://doi.org/10.21577/0103-5053.20170173>
 75. Jiang Z-T, Li R, Liu Y-H (2008) Direct Solid-phase Spectrophotometric Determination of Tartrazine in Soft Drinks Using β -Cyclodextrin Polymer as Support Resin phase spectrophotometry View project Active components in the essential oils View project Direct Solid-phase Spectrophotometric. *J Food Drug Anal* 16:91–96. <https://doi.org/10.38212/2224-6614.2327>
 76. Miller JN (1991) *Basic statistical methods for analytical chemistry. Part 2. calibration and regression methods. A review Analyst* 116:3–14. <https://doi.org/10.1039/AN9911600003>

Publisher's Note Springer Nature remains neutral with regard to jurisdictional claims in published maps and institutional affiliations.

Springer Nature or its licensor (e.g. a society or other partner) holds exclusive rights to this article under a publishing agreement with the author(s) or other rightsholder(s); author self-archiving of the accepted manuscript version of this article is solely governed by the terms of such publishing agreement and applicable law.